Preprints.org

Article

Not peer-reviewed version

# The Anisotropic Etching Mechanism and Morphology Simulation of InP

Hui Zhang *, Lingfei Zhu, Meng Zhu

Posted Date: 6 May 2026

doi: 10.20944/preprints202605.0264.v1

Keywords:

InP; anisotropy; wet etching; etching morphology; Monte Carlo; evolutionary algorithm; simulation

Preprints.org is a free multidisciplinary platform providing preprint service that is dedicated to making early versions of research outputs permanently available and citable. Preprints posted at Preprints.org appear in Web of Science, Crossref, Google Scholar, Scilit, Europe PMC, OpenAlex.

Copyright: This open access article is published under a Creative Commons CC BY 4.0 license, which permit the free download, distribution, and reuse, provided that the author and preprint are cited in any reuse.

Preprints.org (www.preprints.org) | NOT PEER-REVIEWED | Posted: 6 May 2026 doi:10.20944/preprints202605.0264.v1

Disclaimer/Publisher's Note: The statements, opinions, and data contained in all publications are solely those of the individual author(s) and contributor(s) and not of MDPI and/or the editor(s). MDPI and/or the editor(s) disclaim responsibility for any injury to people or property resulting from any ideas, methods, instructions, or products referred to in the content.

*Article*

# The Anisotropic Etching Mechanism and Morphology Simulation of InP

**Hui Zhang [1,3,*], Lingfei Zhu [2] and Meng Zhu [1,4]**

[1] Industrial Perception and Intelligent Manufacturing Equipment Engineering Research Center of Jiangsu Province, Nanjing University of Industry Technology, Nanjing, China
[2] Phoenixcontact (Nanjing) Intelligent Manufacturing Technology, Nanjing, China
[3] The Southeast University, Nanjing, China
[4] Nanjing University of Science and Technology, Nanjing, China
* Correspondence: zhanghui_ccc@163.com

**Abstract**

As a third-generation semiconductor material, indium phosphide (InP) exhibits complex anisotropic etching characteristics, showing significantly varying etching morphologies under different temperature, concentration, and surfactant conditions. This complexity poses challenges in controlling the etching evolution process and predicting its three-dimensional structures. To address the simulation of InP etching structures and surface morphology, this study first establishes an atomic model of the InP etching system and analyzes how different atomic structures influence crystal plane etching rates. Subsequently, based on the microscopic activation energy theory, we propose an atomic remoArticleval determination function (InP-RPF) for InP etching substrates, numerically elucidating the relationship between macroscopic crystal plane etching rates and microscopic atomic removal probabilities. Furthermore, we develop an evolutionary Monte Carlo etching system model (InP-EMC), employing evolutionary algorithms to continuously optimize the energy parameters in the InP-RPF function, thereby adjusting the removal probabilities of various atomic types on the substrate and validating the simulated etching rates. Experimental comparisons demonstrate that the InP-EMC model accurately constrains atomic removal probabilities using limited crystal plane etching rate data, achieving simulation accuracy exceeding 90% for full-crystal-plane etching rates, mask etching structures, and surface morphology characteristics.

**Keywords:** InP; anisotropy; wet etching; etching morphology; Monte Carlo; evolutionary algorithm; simulation

## 1. Introduction

Silicon carbide (SiC), gallium nitride (GaN), indium phosphide (InP), and other crystalline compounds, as third-generation semiconductor materials, have become core substrates for radio frequency (RF) chips, power semiconductors, and optoelectronic chips due to their outstanding resistance to high temperature, high voltage, high frequency, and high-energy radiation, thereby driving the upgrading of semiconductor technology toward higher performance and greater diversity[1–4]. At present, the commonly used methods for micro/nanoscale processing of crystalline materials are dry etching and wet etching [5–7]. Dry etching is a process that utilizes high-energy ion beams to react with or directly bombard the crystal surface to remove the predefined material, enabling the fabrication of trench structures with vertical sidewalls, low lateral undercut, and high aspect ratios. However, the ion bombardment during the etching process degrades the surface quality of the material, and the technique lacks the capability to produce sidewalls with specific inclination angles, resulting in relatively high production costs. Wet etching, in contrast, is an anisotropic

© 2026 by the author(s). Distributed under a Creative Commons CC BY license.

Preprints.org (www.preprints.org) | NOT PEER-REVIEWED | Posted: 6 May 2026 doi:10.20944/preprints202605.0264.v1



chemical process between an etching solution and the material being etched, offering significant advantages for fabricating irregular and complex three-dimensional structures such as sharp corners, cavities, cantilever beams, and non-vertical sidewalls. Nevertheless, the etching rate and the resulting morphology are governed by both the physicochemical properties of the etchant (e.g., solution concentration, diffusion rate, adsorption characteristics) and the atomic structural features of the crystalline material (e.g., substrate crystal orientation, crystal-plane density, atomic species), necessitating extensive experimental validation of the etching evolution process and its outcomes [8–12].

To address the challenges in simulating the etching structures and surface morphology during the wet etching process of InP crystals, this study adopts the following approaches. At the theoretical level, the surface activation energy theory and the double-dangling-bond etching theory are employed to explain, from the perspective of microscopic atomic energy, the origin of the anisotropic etching behavior of InP crystals. Subsequently, the step-flow theory is used to describe the etching evolution process. At the simulation and modeling level, by analyzing the anisotropic etching rate distribution and surface morphology characteristics of InP crystals, combined with the atomic structure features of their crystal planes, a method for defining the atomic states on InP crystal planes is proposed, and a substrate model is constructed. An atomic removal probability function (InP-RPF) is then established for the InP substrate, enabling the classification of etching probabilities for different types of atoms. Furthermore, an Evolutionary Monte Carlo etching system model (InP-EMC) is developed. Through population evolution, the energy parameters in the InP-RPF function are iteratively refined to adjust the removal probabilities of various atomic types on the substrate, thereby gradually approximating the simulated crystal-plane etching rates to the experimental ones. Upon termination of the evolution, the optimized energy parameters of the InP-RPF function are imported into the etching substrate model, allowing the process simulation of three-dimensional etching structures and surface morphologies for wafers with different crystallographic cuts and mask patterns of arbitrary shapes.

## 2. Physicochemical Property Analysis of InP

InP is a III–V compound semiconductor material with a melting point of 1070 °C and a dark gray, pitch-like luster. Its crystal structure is of the zinc blende type, with space group Fd-3m and lattice parameter a = 5.904 Å. In the crystal, the In–P–In and P–In–P bond angles are both 109.47°. When rotated by 90° about the [001] crystallographic direction, the spatial positions of In and P atoms are interchanged [13–15]. The crystal structure of the InP unit cell is shown in Figure 1(a). Studies have shown that in InP crystals, the surface atomic arrangement characteristics differ not only among crystal planes with different orientations but also between the two opposite sides (i.e., the two polar opposite surfaces) of the same crystallographic direction. Furthermore, the types of surface atoms and their relative proportions on each crystal plane also exhibit significant variations. For example, the (111) and ($\bar{1}\bar{1}\bar{1}$) planes are such a pair. Figure 1(b) illustrates the atomic structures of typical crystal planes with different orientations [13,16,17].

© 2026 by the author(s). Distributed under a Creative Commons CC BY license.

Preprints.org (www.preprints.org) | NOT PEER-REVIEWED | Posted: 6 May 2026 doi:10.20944/preprints202605.0264.v1



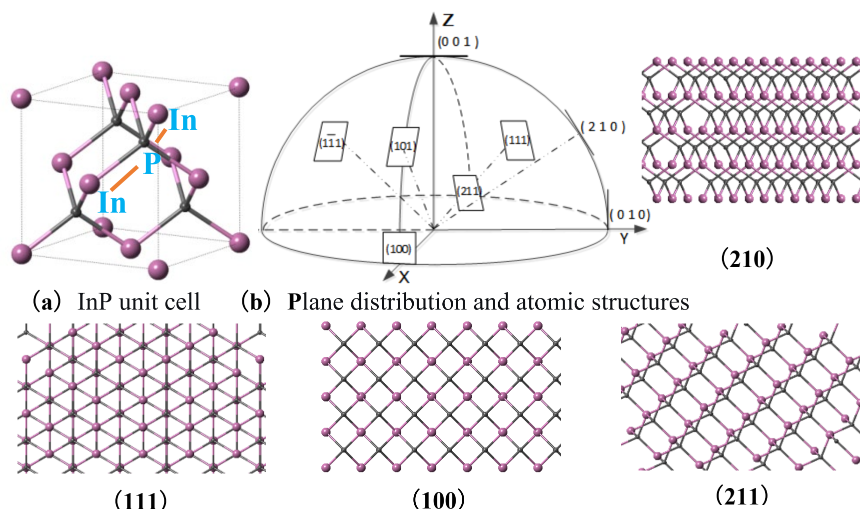


**Figure 1.** InP unit cell and atomic structures of some typical crystal planes.

In industrial production, to obtain smooth and controllable etched surfaces of InP with specific morphologies (e.g., V-grooves), acid-based etching systems such as HCl, HF, and HBr, or special etching systems like $\alpha$-hydroxy acids, are commonly employed. Mask layers are deposited along specific crystallographic orientations (e.g., [100,110,111]) to selectively remove excess material, thereby achieving the desired microstructures. Among these, the design of the mask and the utilization of the differences in etching rates between crystal planes are key to successful microstructure fabrication.

For the HF+$H_2O_2$ etching system, the etching reaction equations for InP are as follows: [13,14,18]

$$\begin{cases} \text{Oxidation}: InP + 2H_2O_2 \rightarrow In_2O_3 + P_2O_5 + 2H_2O \\ \text{Dissolution}: P_2O_5 + 6HF \rightarrow 2HPF_6 + 3H_2O \end{cases} \quad (1.1)$$

The above etching reaction involves two main steps: 1) Oxidation: the oxidant ($H_2O_2$) in the solution oxidizes the InP surface, forming indium oxide ($In_2O_3$) and phosphorus pentoxide ($P_2O_5$).

2) Dissolution: the generated oxides subsequently react with HF to form soluble fluoride complex compounds ($HPF_6$), which are then removed. Due to differences in the types, proportions, and densities of atomic structures on different crystal planes of InP, as well as external factors such as etchant composition, concentration, and temperature, these variations all contribute to the anisotropy observed in etching rates and morphology.

To elucidate the origin of the anisotropic etching rates observed on different crystal planes of InP, this study investigates the phenomenon from the perspective of crystal plane activation energy. Activation energy is defined as the minimum energy required for reactant molecules to transform into activated molecules during a chemical reaction, and it macroscopically determines the reaction rate: the higher the activation energy, the slower the reaction rate, and vice versa. According to the Arrhenius theory of activation energy, the activation energy of a crystal plane is a temperature-independent constant determined solely by the intrinsic atomic structure of the crystal. Consequently, crystal planes with lower activation energy tend to exhibit faster etching rates. Based on the empirical Arrhenius equation for the activation energy-dependent etching rate, a clear relationship between the crystal plane activation energy and its etching rate can be established, as shown below:

$$E_S = RT \cdot (\ln V_0(S) - \ln V(S)) \quad (1.2)$$

In the formula, S denotes the reactive crystal plane; $V(S)$ is the etching rate of the S crystal plane; $V_0(S)$ is the etching coefficient of the S crystal plane; $E_S$ is the activation energy for the chemical reaction on the S crystal plane; R = 8.31 is the molar gas constant; and T = 273.15 + t (°C) is the corrosion temperature.

© 2026 by the author(s). Distributed under a Creative Commons CC BY license.

Preprints.org (www.preprints.org) | NOT PEER-REVIEWED | Posted: 6 May 2026 doi:10.20944/preprints202605.0264.v1



According to Equation (1.2), the activation energy values for various crystal planes of InP can be obtained by substituting the etching rates at different temperatures for the relevant crystal planes in the HCl:H3PO4(5:1) etching solution reported in reference [19], as shown in Figure 2 and Table 1. It can be observed that the fundamental cause of the anisotropic etching rates on different crystal planes of InP is the difference in activation energy among these planes, which essentially arises from the variations in the types and proportions of atomic structures contained in each crystal plane—i.e., the presence of atoms with different bond energies on different crystal planes.

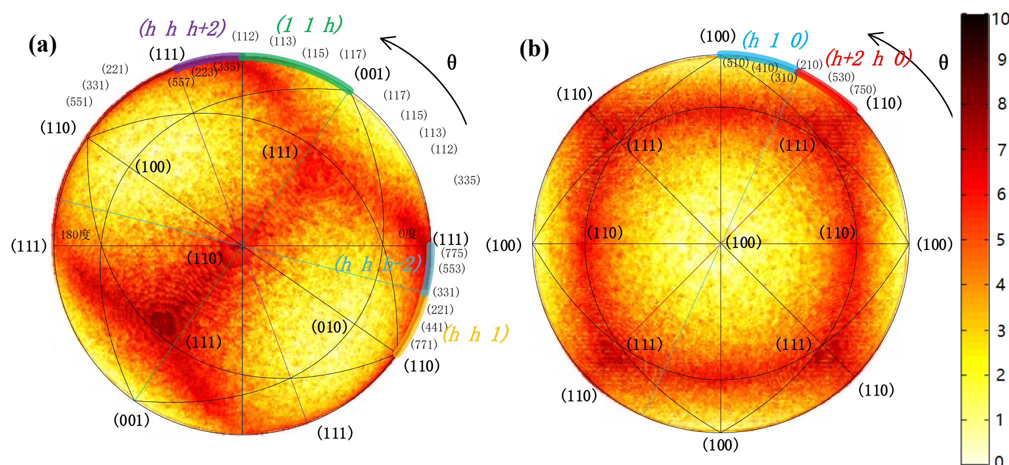

**Figure 2.** Activation energy distribution maps of InP crystal planes: (a) stereographic projection with the [110] central axis; (b) stereographic projection with the [100] central axis.

**Table 1.** Activation energy values of commonly InP planes.

| S | etch rate (um/min) | | | $E_S$ |
|---|---|---|---|---|
| | **10℃** | **20℃** | **40℃** | |
| (100) | 2.5 | 7.9 | 22.5 | 0.35ev |
| (110) | 1.5 | 3.5 | 12.5 | 6.80ev |
| (111) | 1.0 | 4.5 | 11.5 | 7.85ev |
| (211) | 0.1 | 0.3 | 4.0 | 0.71ev |

## 3. The Evolutionary Monte Carlo Model

### *3.1. Etching Analysis of InP Crystals*

Since InP consists of two different types of atoms, In (group III) and P (group V), the surface electronic structures and physicochemical properties of its different crystal planes are distinctly different. For example, the {111} P-terminated plane exhibits higher activity due to a larger number of unsaturated bonds, whereas the {111} In-terminated plane is relatively stable. Moreover, the etching behavior of InP is significantly influenced by electrochemical effects, with etching pores tending to grow along crystallographic directions with faster dissolution rates, thereby forming complex three-dimensional porous structures. Furthermore, by adjusting parameters such as mask orientation, etchant composition, and temperature, InP substrates can achieve richer anisotropic etching morphologies than single-crystal silicon. Figure 3 illustrates the sidewall morphologies of InP trench-masked substrates in different etching solutions.

As can be seen from the figure, when (001) InP substrates are etched with trench masks, different etching solutions result in different sidewall morphologies even with the same mask orientation. Furthermore, when the same etching solution is used but with different mask orientations, distinct sidewall profiles are also observed. In a HBr:$CH_3COOH$ = 1:1 etching solution at 25 °C, for the [110] mask orientation, the sidewalls are left-right symmetric and each consists of two inwardly concave crystal planes, namely {221} and {111}. For the [-110] mask orientation, both sidewalls are also

© 2026 by the author(s). Distributed under a Creative Commons CC BY license.

Preprints.org (www.preprints.org) | NOT PEER-REVIEWED | Posted: 6 May 2026
doi:10.20944/preprints202605.0264.v1



symmetric and are composed solely of {110} planes. In a HCl:$HNO_3$ = 2:1 etching solution at 25 °C, for the [110] mask orientation, the left and right sidewalls consist of vertical {110} planes and inclined {111} planes. For the [-110] mask orientation, both sidewalls are composed of {112} planes making an angle of 35° with the substrate plane. In a HBr etching solution at 25 °C, the sidewalls for both the [110] and [-110] mask orientations are identical, both being {111} planes. These observations indicate that, compared to other crystalline materials such as single-crystal silicon, the anisotropic characteristics of InP, a third-generation semiconductor, are more significantly influenced by the etching environment, exhibiting richer and more distinct etching structures that can meet the fabrication requirements of various chip substrates and sensors.

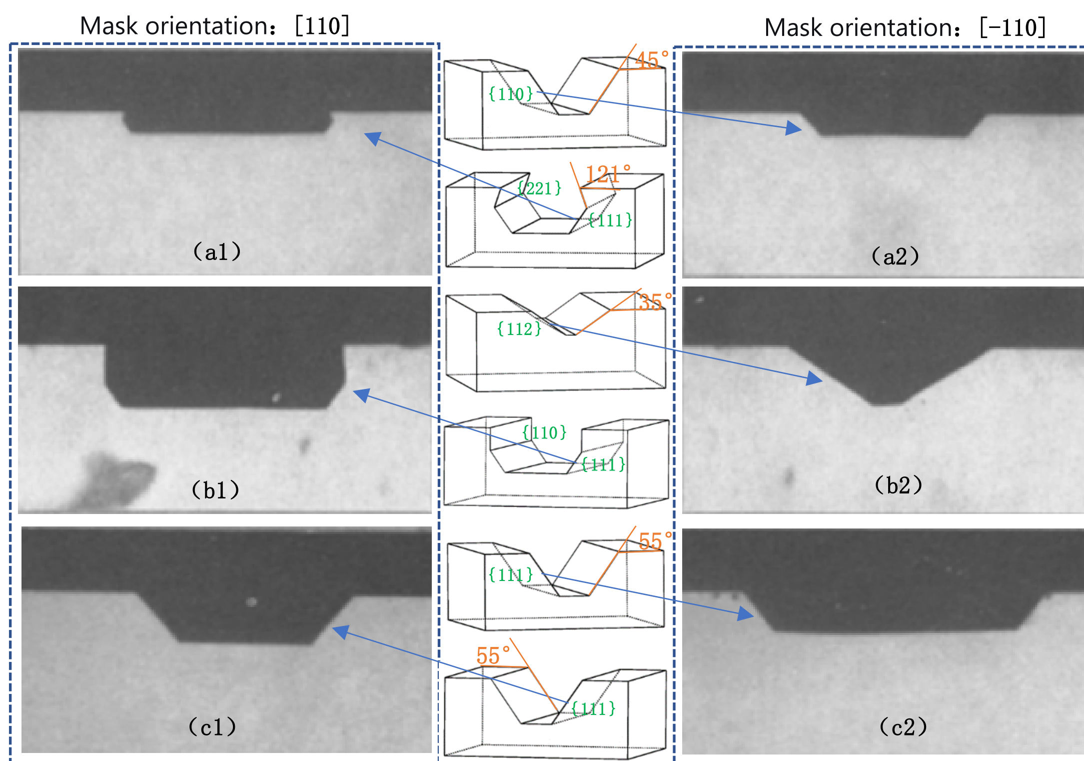


**Figure 3.** Cross-sections of trench sidewalls on (001) InP after 1 min of etching with mask orientations along [110] or [−110]: (a) HBr:$CH_3COOH$ = 1:1 solution at 25 °C; (b) HCl:$HNO_3$ = 2:1 solution at 25 °C; (c) HBr solution at 25 °C [15].

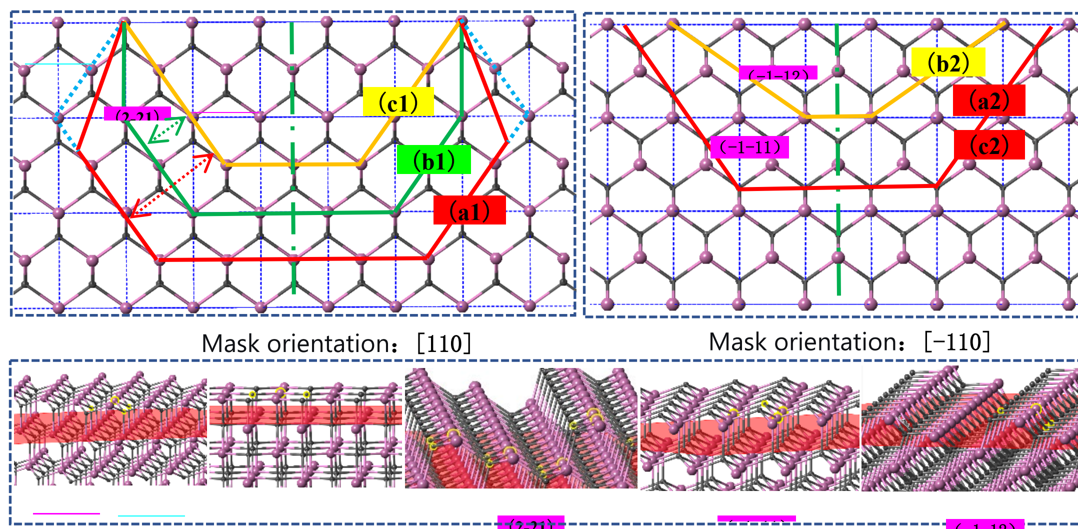


© 2026 by the author(s). Distributed under a Creative Commons CC BY license.

Preprints.org (www.preprints.org) | NOT PEER-REVIEWED | Posted: 6 May 2026
doi:10.20944/preprints202605.0264.v1



**Figure 4.** Atomic structures corresponding to the trench sidewalls in the above figure for (001) InP with mask orientations along [110] and [−110]: (a) HBr:$CH_3COOH$ = 1:1 solution at 25 °C; (b) HCl:$HNO_3$ = 2:1 solution at 25 °C; (c) HBr solution at 25 °C [15].

Although the anisotropic etching behavior of InP crystals can be modulated by the etching environment (e.g., etchant type, concentration, temperature, pH value, etc.), resulting in different morphological features, its fundamental origin remains dependent on the inherent anisotropy of the atomic arrangement and chemical bonding structure of the InP crystal itself. Therefore, to investigate the evolution of anisotropic etching of InP crystals, it is necessary to identify the underlying regularities from their atomic structures and to clarify the characteristics of the atomic types contained in the etch-stop crystal planes. Figure 4 shows the atomic structures of the crystal planes corresponding to the trench sidewalls in Figure 3 for (001) InP with mask orientations along [110] and [−110]. It can be clearly seen from the figure that, although the etching solutions and mask orientations differ, the etch-stop planes are relatively stable, consisting mainly of {111}, {110}, {221}, and {112} crystal planes. The etching rates follow the order: V{112} > V{221} > V{110} > VP{111} > VIn{111}. According to the Wulff-Jacodine etching theory, the etch-stop planes of a trench are determined by the crystal planes that exhibit local minima of the etching rate. Therefore, when the local minimum etching rate of an existing sidewall crystal plane is replaced by that of a surrounding crystal plane, the original sidewall plane disappears and a new sidewall emerges. Consequently, the evolution sequence of the etched sidewalls in Figure 4 is c1 → b1 → a1.

Regarding the atomic structures of the above four types of crystal planes, (-111) and (1-11) are P-terminated {111} planes, whose basic structure consists of a surface P atom chemically bonding to three underlying In atoms (a P-type three-bond configuration). In contrast, (-1-11) is an In-terminated {111} plane, with a basic structure of a surface In atom chemically bonding to three underlying P atoms (an In-type three-bond configuration). The P-terminated {111} and In-terminated {111} planes are opposite sides of the same crystallographic plane, among which the P-terminated {111} plane exhibits higher reactivity and thus a relatively lower etching difficulty. The (-110) and (2-21) planes both contain only the two aforementioned types of atoms, i.e., the P-type and In-type three-bond configurations, but with different proportions. On the (-110) plane, the P-type and In-type atoms are arranged alternately, each accounting for 50%; on the (2-21) plane, the proportion of P-type atoms is 2/3. The (-1-12) plane contains both the P-type three-bond configuration and an In-type two-bond configuration, arranged alternately with each accounting for 50%. Based on the etching rate relationships of the above four groups of crystal planes, it can be inferred that the activation energy of the In-type three-bond configuration is greater than that of the P-type three-bond configuration, and the activation energy of the P-type three-bond configuration is greater than that of other configurations such as the In-type two-bond configuration.

### *3.2. InP Substrate Etching Criteria*

Since InP belongs to the cubic crystal system and its crystal structure is similar to that of single-crystal silicon, in order to distinguish the structural types of In and P atoms on the crystal planes and to establish a correlation between microscopic atomic removal and macroscopic etching rates, this study proposes a diatomic classification model for InP based on the four-index classification method used for single-crystal silicon: In_$(m_{PS}, m_{PB}, n_{InS}, n_{InB})$ , P_$(m_{InS}, m_{InB}, n_{PS}, n_{PB})$. According to this model, based on the chemical bond relationships between the target atom and its neighboring atoms, the neighboring atoms of the atom to be etched are divided into heterogeneous direct neighbors (m) and homogeneous meta-neighbors (n). Those with missing chemical bonds are termed surface neighbors (S), while those without missing bonds are termed bulk neighbors (B) [20,21].

Since the energy barrier that an atom on a crystal plane must overcome to detach from the crystal surface during the etching process is closely related to the bond energies between the atom and its neighbors, the molecular bond energy theory can be employed to assess the difficulty of removing a

© 2026 by the author(s). Distributed under a Creative Commons CC BY license.

given atom in the etching reaction based on the number of neighbor atoms of each type. In fact, as long as the removal probabilities of all types of atoms on the crystal plane to be etched are appropriately assigned, the macroscopic etching rate and surface morphology of the crystal plane can be effectively simulated. Based on the target atom type and its bond energy relationships with neighboring atoms, this study defines the atomic removal probability function for the InP etching substrate, designated as the InP-RPF, as follows:

$$P(\mathrm{InP})\begin{cases} P(\mathrm{In})=\begin{cases} P(m_{\mathrm{PS}},m_{\mathrm{PB}},n_{\mathrm{InS}},n_{\mathrm{InB}})=U_{\mathrm{In}}\cdot P(m_{\mathrm{PS}},m_{\mathrm{PB}})\cdot P(n_{\mathrm{InS}},n_{\mathrm{InB}}) \\ P(m_{\mathrm{PS}},m_{\mathrm{PB}})=(1+e^{-\beta E_{\mathrm{In1}}})/(1+e^{\beta*(\varepsilon_{\mathrm{In1}}\cdot m_{\mathrm{PS}}+\varepsilon_{\mathrm{In2}}\cdot m_{\mathrm{PB}}-E_{\mathrm{In1}})}) \\ P(n_{\mathrm{InS}},n_{\mathrm{InB}})=(1+e^{-\beta E_{\mathrm{In2}}})/(1+e^{\beta*(\varepsilon_{\mathrm{In3}}\cdot n_{\mathrm{InS}}+\varepsilon_{\mathrm{In4}}\cdot n_{\mathrm{InB}}-E_{\mathrm{In2}})}) \end{cases} \\ P(\mathrm{P})=\begin{cases} P(m_{\mathrm{InS}},m_{\mathrm{InB}},n_{\mathrm{PS}},n_{\mathrm{PB}})=U_{\mathrm{P}}\cdot P(m_{\mathrm{InS}},m_{\mathrm{InB}})\cdot P(n_{\mathrm{PS}},n_{\mathrm{PB}}) \\ P(m_{\mathrm{InS}},m_{\mathrm{InB}})=(1+e^{-\beta E_{\mathrm{P1}}})/(1+e^{\beta*(\varepsilon_{\mathrm{P1}}\cdot m_{\mathrm{InS}}+\varepsilon_{\mathrm{P2}}\cdot m_{\mathrm{InB}}-E_{\mathrm{P1}})}) \\ P(n_{\mathrm{PS}},n_{\mathrm{PB}})=(1+e^{-\beta E_{\mathrm{P2}}})/(1+e^{\beta*(\varepsilon_{\mathrm{P3}}\cdot n_{\mathrm{PS}}+\varepsilon_{\mathrm{P4}}\cdot n_{\mathrm{PB}}-E_{\mathrm{P2}})}) \end{cases} \end{cases} \tag{2.1}$$

Specifically, $\beta = 1/K_B T$, where $K_B = 8.617 \times 10^{-5}\ eV \cdot K$ is the Boltzmann constant and T is the absolute temperature. The expressions $\varepsilon_{\mathrm{In1}}$ ($\varepsilon_{\mathrm{P1}}$)and $\varepsilon_{\mathrm{In2}}$ ($\varepsilon_{\mathrm{P2}}$) represent the binding energies between the target atom In(P) and its direct surface neighbors and direct substrate neighbors, respectively; $\varepsilon_{\mathrm{In3}}$ ($\varepsilon_{\mathrm{P3}}$)and $\varepsilon_{\mathrm{In4}}$ ($\varepsilon_{\mathrm{P4}}$) denote the binding energies between In(P) and its meta-surface neighbors and meta-substrate neighbors; $E_{\mathrm{In1}}$ ($E_{\mathrm{P1}}$)and $E_{\mathrm{In2}}$ ($E_{\mathrm{P2}}$) indicate the threshold energies between In(P) and its direct neighbors and meta-neighbors; while $U_{\mathrm{In}}$ ($U_{\mathrm{P}}$) is the pre-exponential factor quantifying the external etching environment's influence on the etching probability of In(P) atoms. All energy parameters are expressed in joules (J), with 1eV≈$1.602\times10^{-19}$J.

This function first classifies the etching behaviors of In and P atoms separately. It then correlates, from an energetic perspective, the target atom with its surrounding direct and meta, surface and bulk neighbor atoms to assess the stability of the target atom and describes its etching reaction as a probabilistic event. The function assumes that under fixed etching conditions, the binding energies reflecting the interatomic energy relationships are constant. Consequently, the fundamental reason why different crystal planes exhibit anisotropic etching characteristics lies in the types and proportions of atoms inherently present on each crystal plane. In other words, the InP-RPF function serves as a bridge that establishes the relationship between the macroscopic etching rate of an InP crystal plane and the microscopic atomic removal probability. Once the values of the 12 energy parameters and two pre-exponential factors in the function are determined, the etching probability of any atom on its respective crystal plane can be obtained, ultimately enabling the simulation of crystal plane etching rates and morphologies.

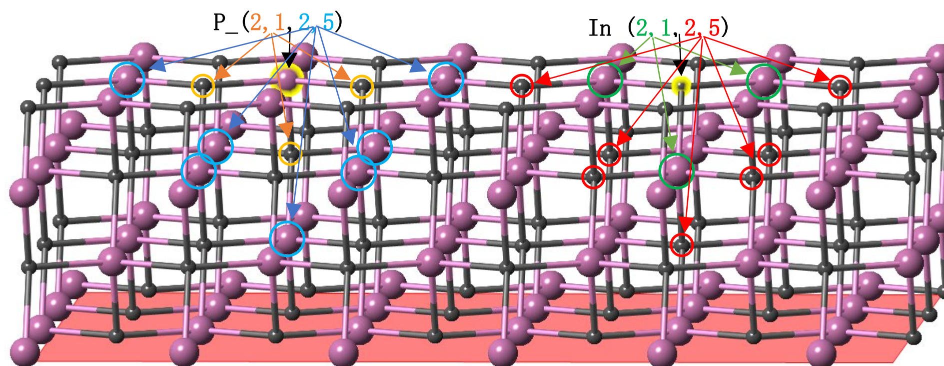


**Figure 5**. Schematic diagram of atomic classification on the etching substrate using the diatomic classification model of InP.

© 2026 by the author(s). Distributed under a Creative Commons CC BY license.

Preprints.org (www.preprints.org) | NOT PEER-REVIEWED | Posted: 6 May 2026 doi:10.20944/preprints202605.0264.v1



### 3.3. The InP-EMC Model

To construct the Evolutionary Monte Carlo (EMC) etching simulation model, this study performed structural simulations of InP substrate etching in a HBr:$CH_3COOH$ = 1:1 solution at 25℃. Four typical crystal planes, namely (100), (110), (111), and (211), were selected as simulation targets, among which the (100) plane served as the rate-calibration plane and the other three as the rate-simulation planes. The energy parameters were automatically adjusted using an evolutionary algorithm to fit the MC model to the experimental data. The experimental etching rates and the MC-simulated etching rates for the above crystal planes are denoted as $v_i$ and $v_{MC(i)}$, respectively, where $i = 1,2,3$ indexes the crystal planes. The individual fitness function is then expressed as:

$$\begin{cases} min \quad f_{sum} = \sum f_1 + f_2 + f_3 \\ f_i = \left| v_i - v_{MC(i)} \right| \\ i = 1,2,3 \end{cases} \tag{2.2}$$

That is, the objective is to minimize the sum of the errors between the experimental etching rates and the MC-simulated etching rates. The smaller the value $f_{sum}$, the closer the simulation results are to the experimental values.

The evolutionary termination condition is set as follows:

$$\begin{cases} \eta = \dfrac{f_{sum}}{v_{sum}} \le \mathrm{K} \\ v_{sum} = \sum v_{e(1)} + v_{e(2)} + v_{e(3)} \end{cases} \tag{2.3}$$

That is, when the ratio η of the errors sum of the MC-simulated rates to the sum of experimental rates is less than or equal to K∈[0,1], the evolution is terminated and the simulation is completed. In this study, K is set to 0.10. Table 2 lists the assignment of the reference planes for the four sample crystal planes and the initial surface atomic type compositions of each crystal plane. Figure 6 shows the process flow of the InP-EMC etching simulation model.

**Table 2.** Initial surface atomic type compositions of the sample planes.

| **Smaple plane** | | **Calibration planes** | **Constraint planes** | | |
|---|---|---|---|---|---|
| | | **(100)** | **(110)** | **(111)** | **(211)** |
| In ($m_{PS}$,$m_{PB}$,$n_{InS}$,$n_{InB}$) | 1 | 0,2,4,4 | 2,1,2,5 | 0,3,6,3 | 1,1,0,5 |
| | 2 | \ | \ | \ | \ |
| P ($m_{InS}$,$m_{InB}$,$n_{PS}$,$n_{PB}$) | 3 | \ | 2,1,2,5 | \ | 1,2,3,3 |
| | 4 | \ | \ | \ | 0,3,5,4 |

© 2026 by the author(s). Distributed under a Creative Commons CC BY license.

Preprints.org (www.preprints.org) | NOT PEER-REVIEWED | Posted: 6 May 2026 doi:10.20944/preprints202605.0264.v1



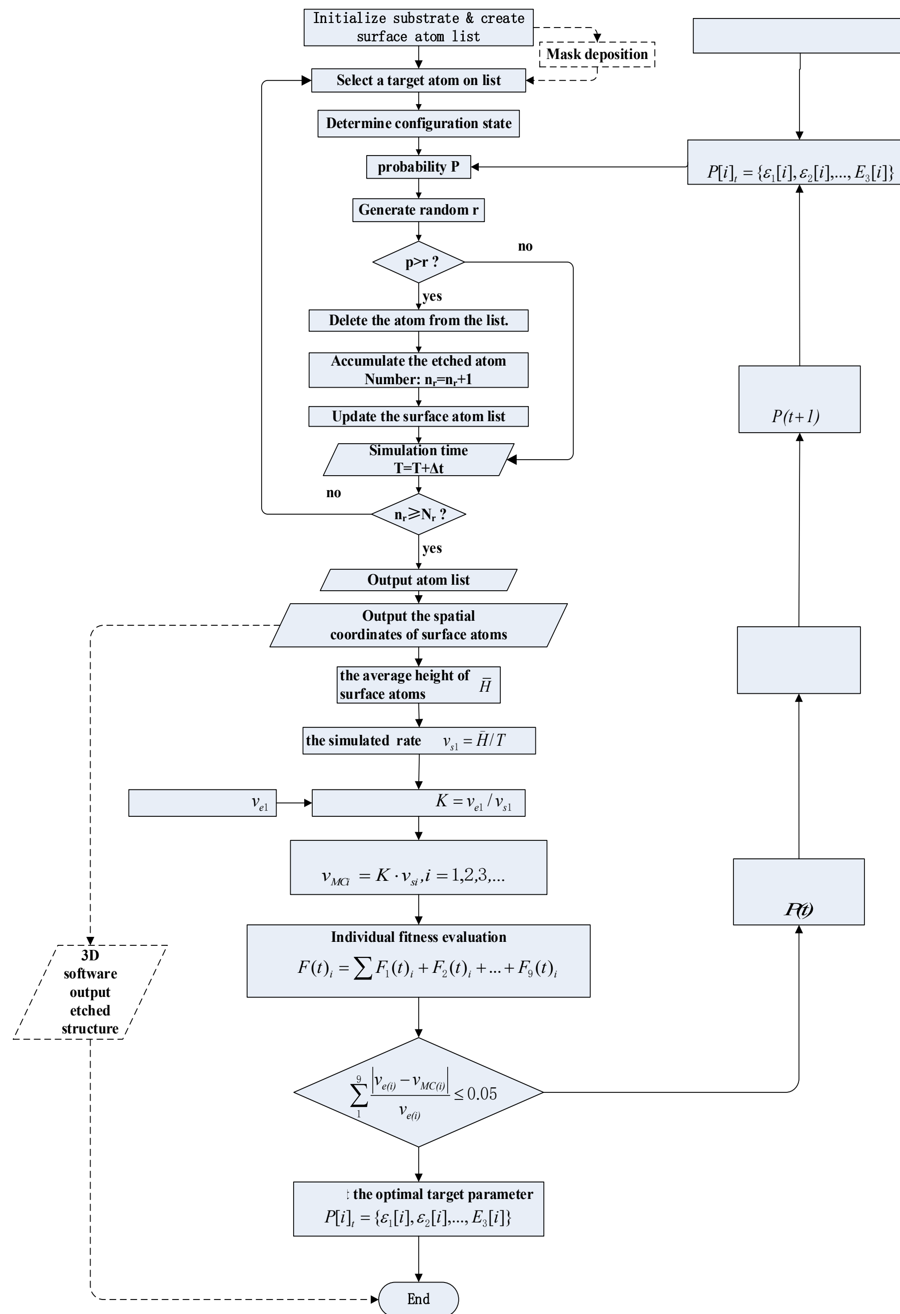


**Figure 6.** The InP-EMC etching process model flowchart.

According to the process flow of the InP-EMC etching simulation model illustrated in Figure 6, a genetic evolution population $P(t)=\{P[1],P[2],...,P[30]\}^T$ is established for the target optimization parameters ( $\varepsilon_1$ , $\varepsilon_2$ , $\varepsilon_3$ , $\varepsilon_4$ , $E_1$ , $E_2$ ). Subsequently, evolutionary selection is performed on the parameters of the etching probability function (Equation 2.1) using the fitness evaluation criterion (Equation 2.2), until the evolution results satisfy the termination condition (Equation 2.3). Figure 5 shows the population fitness evolution curve at the termination of the optimization model after 115 generations of evolution under the etching conditions of HBr:$CH_3COOH$ = 1:1 at 25 °C.

© 2026 by the author(s). Distributed under a Creative Commons CC BY license.

Preprints.org (www.preprints.org) | NOT PEER-REVIEWED | Posted: 6 May 2026 doi:10.20944/preprints202605.0264.v1



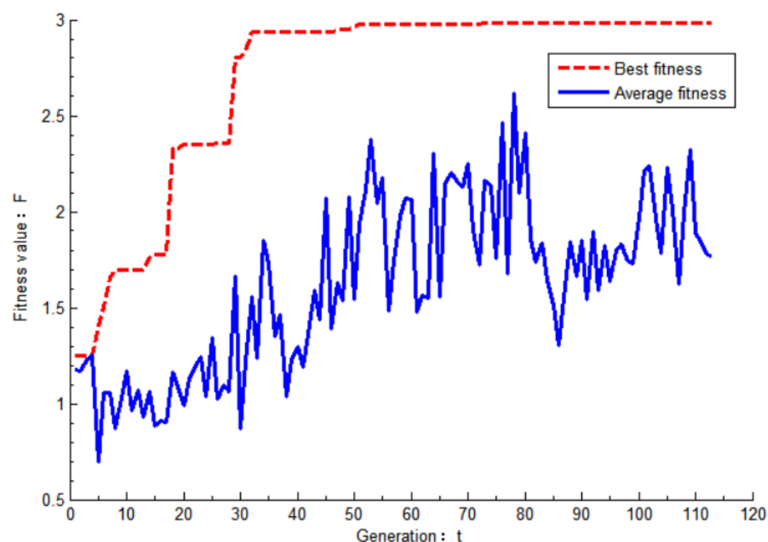


**Figure 7. Genetic evolution process of the EMC etching simulation model.**

As shown in Figure 7, in the first generation of the evolutionary population, both the average fitness value and the best fitness value were relatively low, approximately 1.25. As evolution proceeded, the average fitness value exhibited a fluctuating upward trend and maintained significant oscillations around 1.8, while the best fitness value increased rapidly—showing a stepwise rise from generation 1 to generation 35, followed by a gradual increase, reaching 2.95 at generation 115, thereby meeting the evolutionary termination condition. This indicates that the evolutionary algorithm can rapidly select the optimal individuals and ensure that population evolution proceeds quickly in the direction required by the fitness function. Moreover, the large fluctuations in the average fitness value demonstrate that, in each generation, the population retains outstanding individuals from the previous generation and continuously generates numerous new individuals through mutation, thereby preserving population diversity and preventing premature convergence. Once the evolutionary termination condition is satisfied, the program automatically terminates and outputs the optimal values of the etching probability function parameters and the simulated etching rates of the calibration crystal planes. At this stage, the average error of the simulated etching rates is within 10%. The output results of the target optimization parameters and the simulated etching rates of the calibration crystal planes at the termination of evolution are presented in Table 3.

**Table 3.** Genetic evolution output results of the EMC etching optimization model Unit: μm.

| **Optimization results** | $\varepsilon_{In1}$=0.336 $\varepsilon_{In2}$=0.382 $\varepsilon_{In3}$=0.247 $\varepsilon_{In4}$=0.089 $E_{In1}$=0.790 $E_{In2}$=1.20 $U_{In}$=143.8 | | | |
|---|---|---|---|---|
| | $\varepsilon_{P1}$=0.477 $\varepsilon_{P2}$=0.440 $\varepsilon_{P3}$=0.045 $\varepsilon_{P4}$=0.347 $E_{P1}$=1.03 $E_{P2}$=1.76 $U_{P}$=96.2 | | | |
| Crystal Planes | (100) | (110) | (111) | (211) |
| Experimental rate | 7.90 | 0.400 | 0.350 | 3.500 |
| Simulated rate | 7.90 | 0.401 | 0.333 | 3.500 |

© 2026 by the author(s). Distributed under a Creative Commons CC BY license.

Preprints.org (www.preprints.org) | NOT PEER-REVIEWED | Posted: 6 May 2026
doi:10.20944/preprints202605.0264.v1



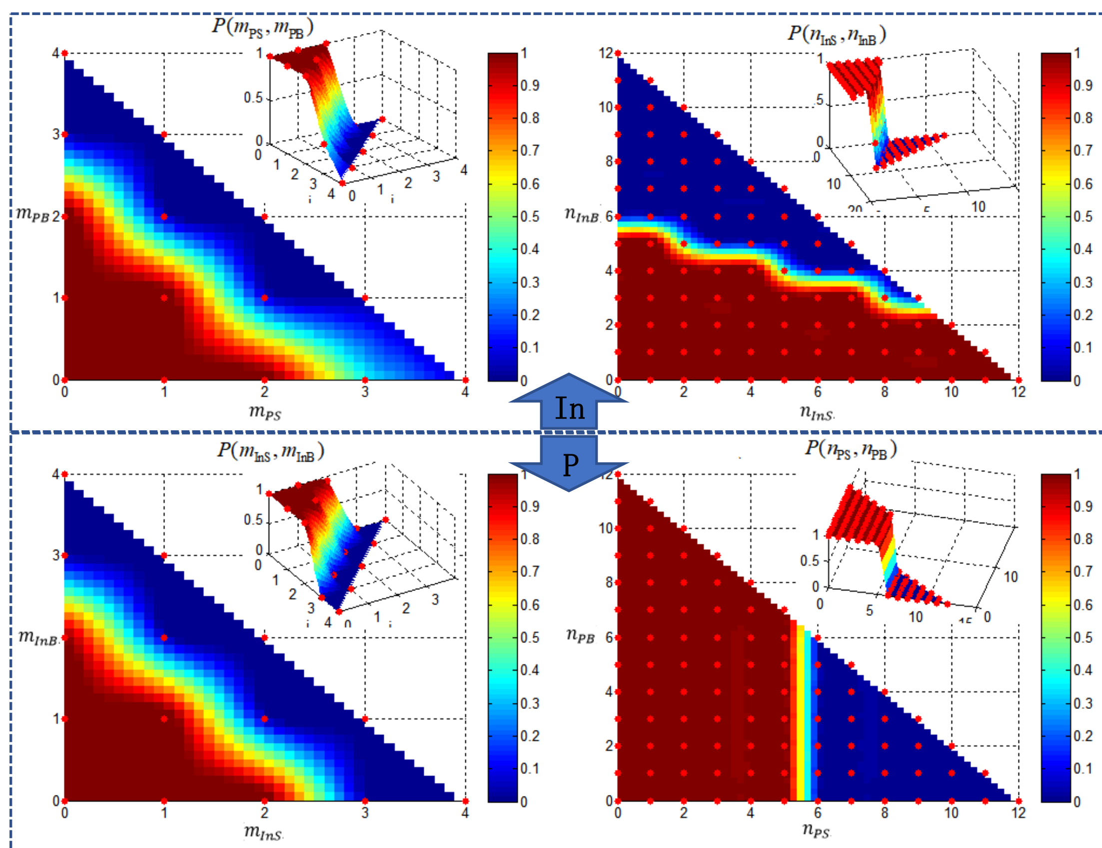


**Figure 8.** Relationship between the removal probability P of the target atom and its neighboring atoms: In_($m_{PS}$, $m_{PB}$)、In_($n_{InS}$, $n_{InB}$)、P_($m_{InS}$, $m_{InB}$)、P_($n_{PS}$, $n_{PB}$).

Figure 8 illustrates the respective effects of the direct neighbors In_($m_{PS}$, $m_{PB}$) and meta-neighbors In_($n_{InS}$, $n_{InB}$) of In atoms, as well as the direct neighbors P_($m_{InS}$, $m_{InB}$) and meta-neighbors P_($n_{PS}$, $n_{PB}$) of P atoms, on the etching probability under the conditions of 25 °Cand a HBr:$CH_3COOH$ = 1:1 solution. It can be seen from the figure that when the neighbor atomic types are distributed in the blue region, the removal probability is low; when distributed in the red region, the removal probability is high; and when distributed in the intermediate transition zone, the removal probability is medium. In the etching probability function (Equation 2.1), $P(m_{PS}, m_{PB})$ and $P(n_{InS}, n_{InB})$ must act together to determine the etching probability of an In atom, following an "AND" logic: (1) if both components correspond to a high removal probability, the overall removal probability is high; (2) if either component is associated with a medium or low removal probability, the overall removal probability is medium or low. The same rule applies analogously to $P(m_{InS}, m_{InB})$ and $P(n_{PS}, n_{PB})$ for P atoms. Therefore, according to the formula for calculating the number of neighbor types:

$$\begin{cases} \text{In: } \mathrm{N}(m_{PS}, m_{PB}, n_{InS}, n_{InB}) = \mathrm{N}(m_{PS}, m_{PB}) \cdot \mathrm{N}(n_{InS}, n_{InB}) \\ \text{P: } \mathrm{N}(m_{InS}, m_{InB}, n_{PS}, n_{PB}) = \mathrm{N}(m_{InS}, m_{InB}) \cdot \mathrm{N}(n_{PS}, n_{PB}) \end{cases} \quad (2.4)$$

Based on the calculation, the number of surface atomic types for both In and P atoms in the InP crystal is 1,170 (15*78). Among these, In atoms exhibit 288 types (6*48) with a high removal probability and 882 types with a medium or low removal probability. For P atoms, 342 types (6*57) have a high removal probability, and 828 types have a medium or low removal probability. From a statistical probability perspective, it can be concluded that P atoms are more readily removed than In atoms during the etching reaction.

© 2026 by the author(s). Distributed under a Creative Commons CC BY license.

Preprints.org (www.preprints.org) | NOT PEER-REVIEWED | Posted: 6 May 2026 doi:10.20944/preprints202605.0264.v1



## 4. EKMC Simulation Analysis

### 4.1. Effect of Microscopic Atomic Activation Energy on Etching Anisotropy

According to the crystal activation energy theory, together with Equation (1.2) and the method for calculating the simulated crystal plane etch rate, the following equation is derived:

$$\begin{cases} \frac{1}{n}\sum_{i=1}^{n}\frac{P_i \cdot h_i}{\Delta t_i} = V_0(S)\cdot \exp(-E_S / RT) \\ E_S = NA \cdot E_a \ \& \ R = NA \cdot k_B \end{cases} \quad (3.1)$$

Rearranging the equation yields:

$$P = V_0(S)\cdot e^{-E_a/k_B T} \Big/ \frac{1}{n}\sum_{i=1}^{n}\frac{h_i}{\Delta t_i} \quad (3.2)$$

Taking the logarithm of both sides of the above equation and rearranging the variables yields the formula for calculating the surface atomic activation energy.

$$E_a(m,m,n,n) = k_B T \cdot (\ln(A) - \ln(P(m,m,n,n))) \quad (3.3)$$

Where $A = V_0(S) \Big/ \frac{1}{n}\sum_{i=1}^{n}\frac{h_i}{\Delta t_i}$ is the pre-exponential factor; $(m,m,n,n)$ denotes the structural type of the In or P atom; $N$ is the number of surface atoms; $P_i$ is the removal probability of the $i$-th atom in the surface atom list; $\Delta t$ is the time interval between two adjacent etching events; $E_a$ is the microscopic atomic activation energy; $NA$≈6.02×1023 is Avogadro's constant; $k_B$≈1.3806505×10-23J/K is Boltzmann's constant. All energy parameters are expressed in joules (J), with 1eV≈1.602×10-19J.

Based on the above equation, the relationship between the microscopic atomic activation energy of InP crystals and the corresponding removal probability P in the 25℃ HBr:CH3COOH = 1:1 solution can be obtained, as shown in Figure 9. It is evident from the figure that the atomic activation energy of InP is inversely proportional to its removal probability P : the higher the removal probability, the lower the atomic activation energy. Therefore, crystal planes with a low etching rate exhibit relatively high activation energies, indicating that the constituent atoms possess larger activation energies; conversely, crystal planes with a high etching rate have smaller activation energies, implying that the constituent atoms possess smaller activation energies. In other words, the anisotropic etching behavior of InP originates from the heterogeneous distribution of atoms with different activation energies across various crystal planes. When the activation energy of an atom is higher and its proportion on a given crystal plane is larger, the overall activation energy of that plane increases, leading to a lower etching probability for the atoms. Conversely, when the activation energy is lower and the proportion of such atoms is smaller, the crystal plane activation energy decreases, resulting in a higher etching probability.

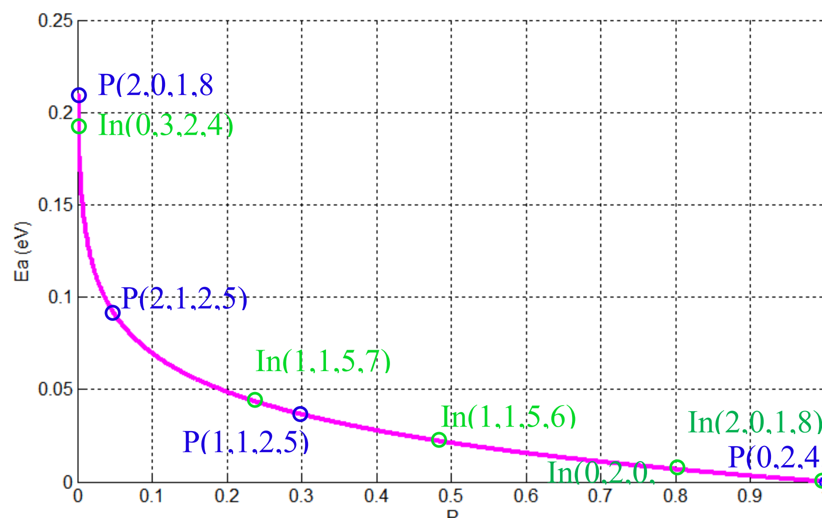


© 2026 by the author(s). Distributed under a Creative Commons CC BY license.

**Figure 9.** Correspondence between the microscopic atomic activation energy and the removal probability P for InP crystals.

*4.2. Hemispherical Crystal Plane Etching Rate Analysis*

Based on the Monte Carlo etching simulation method, a spherical InP crystal substrate model with a diameter of 250 unit cells and no mask on the surface was constructed. Substituting the optimized parameters from Table 3, the etching simulation results for four etching stages under a HBr:$CH_3COOH$ = 1:1 solution at 25℃were obtained, as shown in Figure 10(a). Meanwhile, based on the depth difference of the crystal sphere before and after etching, the etching rate distribution maps of the hemispherical crystal planes for the [100] and [110] central axes were obtained, as shown in Figure 10(b-c). According to the Wulff-Jaccodine etching theory, the wet etching of a spherical crystalline material can be regarded as convex corner etching, i.e., the etched structure of the sphere is composed of fast-etching planes. Analysis of the etching results at different stages in Figure 10(a) shows that after a period of etching, the crystal sphere forms a relatively regular tetrahedron. Combined with Figure 10(b-c), it can be seen that all four faces are (100) planes. From Figure 10(b-c), for the [100] central axis, the etching rate distribution of InP exhibits four-fold central symmetry. The fastest etching rate occurs mainly at the axis center and the coordinate axis vertices, i.e., the (100) plane, at approximately 8.5 μm/min. The slowest etching rate is concentrated near the vertices of the dashed quadrilateral, i.e., the (111) plane, at approximately 2.3 μm/min. For the [110] central axis, the etching rate distribution shows mirror symmetry with respect to the Y-axis. The fastest etching rates are mainly located on both sides of the axis and at the Y-axis vertex, i.e., the (100) plane. The slowest etching rates are concentrated in the front and rear sections of the Y-axis, i.e., the (111) plane.

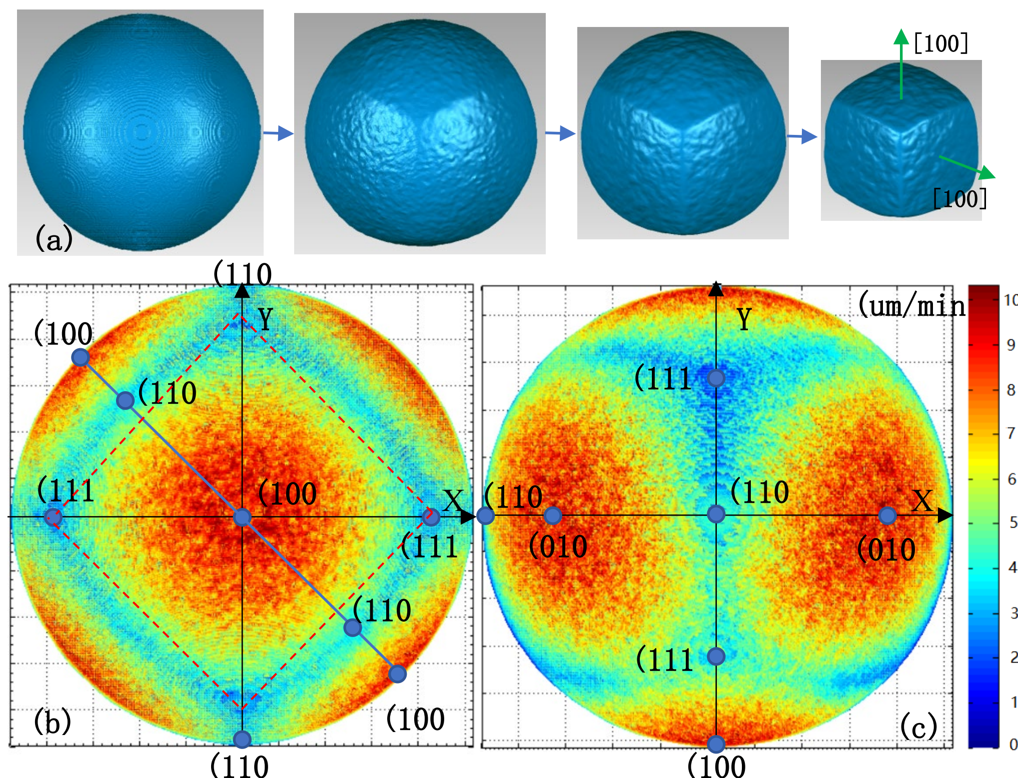


**Figure 10.** Etching results of an InP sphere under 25 °C HBr:$CH_3COOH$ = 1:1 solution: (a) etching results at different stages; (b) etching rate distribution map of hemispherical planes with the [100] central axis; (c) etching rate distribution map of hemispherical planes with the [110] central axis.

Figure 11 shows the simulated etching rates calculated from the points taken on the hemispherical profile lines of the InP crystal for the [100] and [110] central axes, based on the etching rate distribution maps of the hemispherical crystal planes in Figure 10(b-c). For the [100] central axis,

© 2026 by the author(s). Distributed under a Creative Commons CC BY license.

doi:10.20944/preprints202605.0264.v1



on the (111)–(100)–(111) profile line, the rate curve is dome-shaped, with the maximum rate occurring on the (100) plane and the minimum rate on the (111) plane. On the (110)–(100)–(110) profile line, the rate curve exhibits a"W"shape, with the maximum rates at the three apex points, i.e., the (100) planes, and the minimum rates at the two bottom points, i.e., the (110) planes. For the [110] central axis, on the (010)–(110)–(010) profile line, the rate curve is "M"shaped, with the maximum values on the two vertex planes, i.e., the (100) planes, and the minimum values on the three bottom planes, i.e., the (110) planes. On the (111)–(110)–(111) profile line, the rate curve is approximately "W"shaped; the maximum rates occur on the (100) planes at the two ends, while the etching rates on the two bottom (111) planes of the "W"also differ. Specifically, the rate on the (111)-A plane is lower than that on the (111)-B plane. This difference arises because the atomic arrangements on the two opposite sides of the (111) plane are different: the A side is In-terminated, with a surface In atom bonded to three underlying P atoms, whereas the B side is P-terminated, with a surface P atom bonded to three underlying In atoms. Since In atoms are more difficult to etch than P atoms, the etching rate of the (111)-A plane is lower than that of the (111)-B plane. Table 4 compares the simulated etching rates of several typical crystal planes with the experimental data. The maximum relative error is less than 8%, indicating high simulation accuracy.

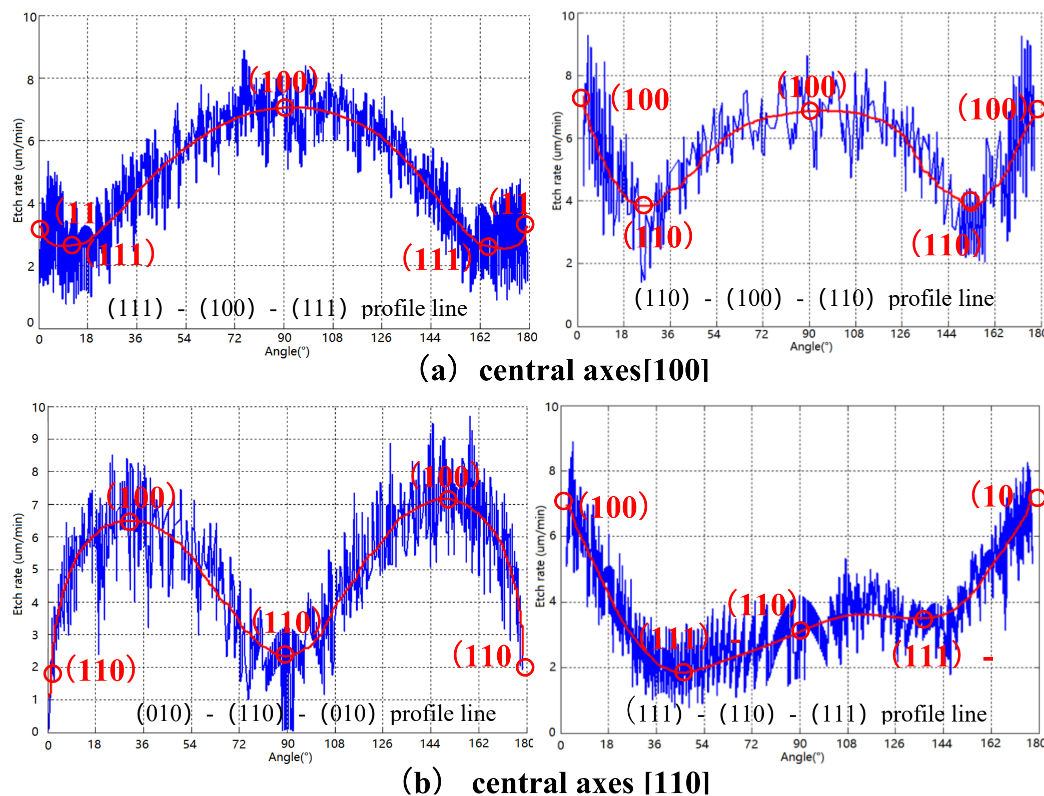


**Figure 11.** Simulated etch rates of crystal planes on the InP hemispherical profile lines with central axes of (a) [100] and (b) [110] under 25 °C HBr:$CH_3COOH$ = 1:1 solution.

**Table 4.** Comparison of simulated and experimental rates of crystal planes in a 25 °C HBr:$CH_3COOH$ = 1:1 solution (μm/min).

| Crystal Plane | (100) | (110) | (111) | (211) | (221) | (411) | (310) |
| --- | --- | --- | --- | --- | --- | --- | --- |
| Experimental rate Vs | 7.90 | 0.400 | 0.350 | 3.500 | 3.45 | 6.65 | 5.35 |
| Simulated rate Vm | 7.20 | 0.401 | 0.333 | 3.500 | 3.65 | 6.15 | 4.98 |
| Relative error | 0.00% | 2.50% | 4.86% | 0.00% | 5.78% | 7.82% | 6.92% |

© 2026 by the author(s). Distributed under a Creative Commons CC BY license.

*4.3. 3D Etching Morphology Analysis*

In principle, the InP-EMC etching simulation model developed in this study is capable of simulating etching processes on different crystal plane substrates with arbitrary mask shapes under any etching conditions. Prior to use, only the experimental etching rates of the (100), (110), (111), and (211) crystal planes under the desired etching conditions are required.

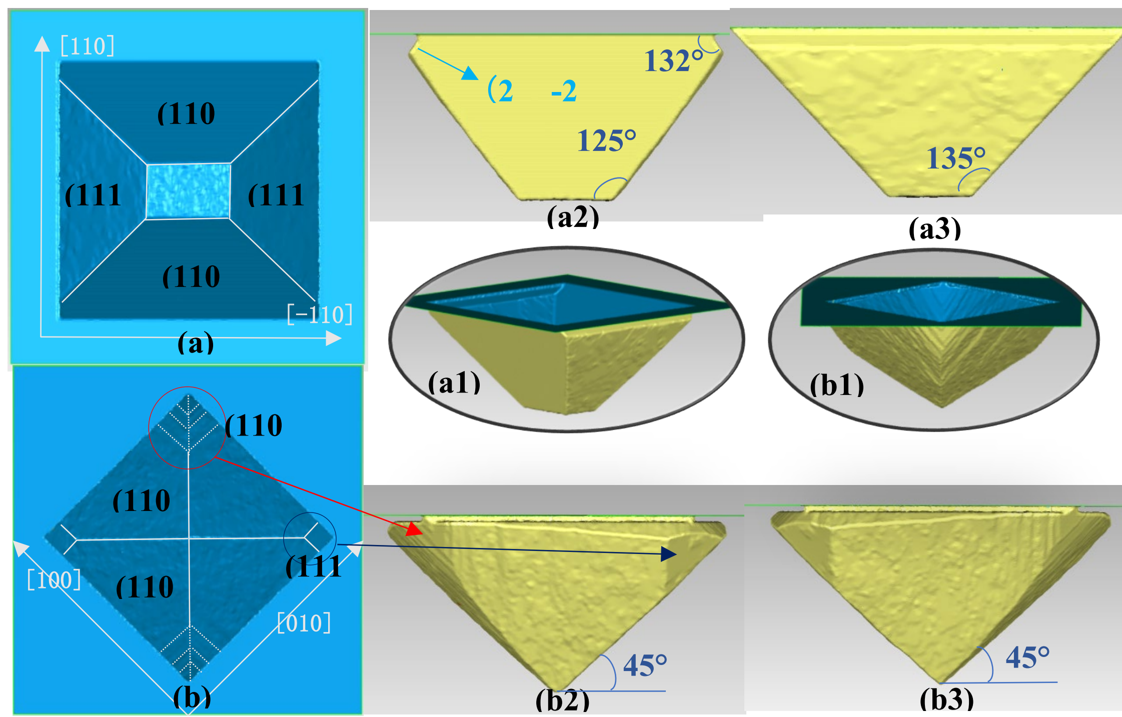


**Figure 12. Simulation results of square and rhombus trench mask etching using the InP-EMC simulation model in a 25 °C HBr:$CH_3COOH$ = 1:1 solution.**

The figure above shows the simulated etching results of square mask structures on a (100) substrate with mask edges oriented along different directions under a HBr:$CH_3COOH$ = 1:1 solution at 25 °C. In Figure 12(a), when the mask edge is oriented along the [110] direction, the sidewalls consist of (2-21) and (111) crystal planes; when oriented along the [-110] direction, the sidewalls consist solely of (110) crystal planes. Moreover, the microscopic surface morphology of the etched crystal planes is successfully visualized. Comparison with the experimental etching results in Figure 3(a) shows perfect agreement in the sidewall angles, validating the accuracy and reliability of the simulation model under this etching system. Further examination of the rhombus mask results in Figure 12(b) reveals that, for different crystal orientations, the sidewall crystal planes are all (110), and two types of small sidewalls appear at the corners, namely densely packed (110) planes and single (111) planes.

© 2026 by the author(s). Distributed under a Creative Commons CC BY license.

Preprints.org (www.preprints.org) | NOT PEER-REVIEWED | Posted: 6 May 2026 doi:10.20944/preprints202605.0264.v1



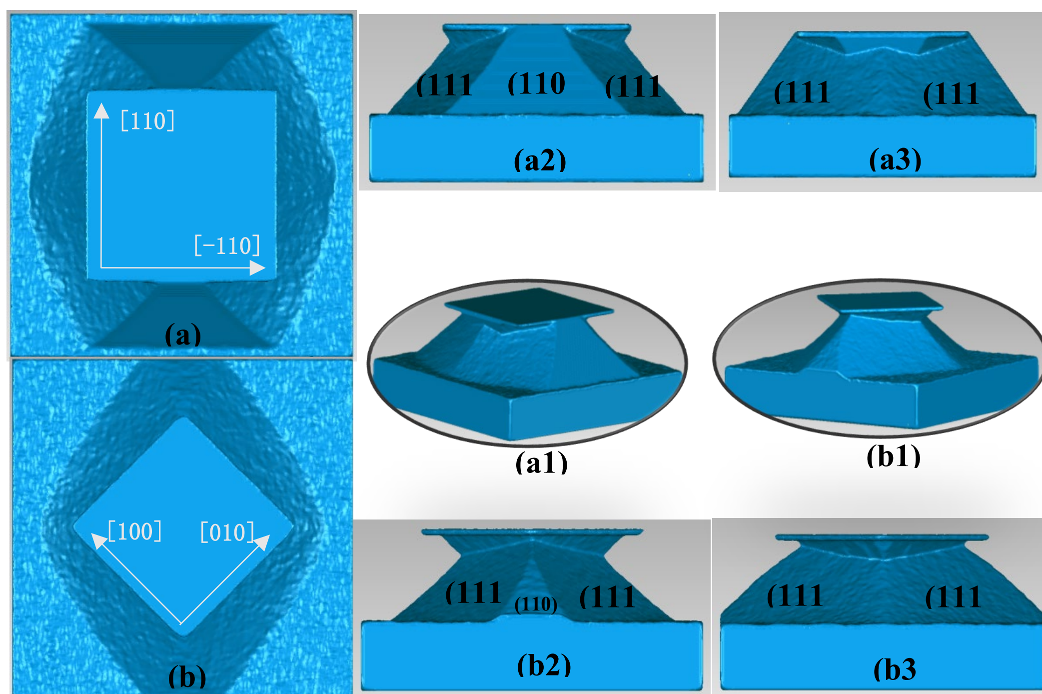


**Figure 13.** Simulation results of square and rhombus mesa mask etching using the InP-EMC simulation model in a 25 °C HBr:$CH_3COOH$ = 1:1 solution.

The above figure shows the simulated etching results of a square mesa mask on a (100) substrate with different mask edge orientations under a HBr:$CH_3COOH$ = 1:1 solution at 25 °C. The etched sidewalls of the square mesa mask consist of six crystal planes. When the mask edge is oriented along the [110] direction, the sidewalls are composed of (111) and (110) planes; when oriented along the [−110] direction, the sidewalls contain only (111) planes (as shown in Figure 13(a)). Further observation of the etched results of the rhombus mask in Figure 13(b) reveals that the etched sidewall planes are exactly the same as those in Figure 13(a), with only differences in the sizes of the constituent crystal planes. Thus, for mesa etching, as long as the etching time is sufficiently long, the final etched sidewall planes consist of the same set of crystal planes regardless of the mask shape. These simulation results demonstrate that the InP-EMC etching simulation model can not only reproduce macroscopic structures and reflect surface morphology states, but also accurately capture the corner rounding features at the intersections of sidewalls in the corner regions, further proving the model's predictive capability for complex three-dimensional etched morphologies.

## 5. Conclusions

In this paper, an InP-EMC etching simulation model based on the Evolutionary Monte Carlo method were constructed for the wet etching process of InP. The microscopic mechanism of etching anisotropy was systematically analyzed, and simulation validation of etching rates on different crystal planes as well as three-dimensional etching morphologies was accomplished. The results show that the essence of the anisotropic wet etching of InP lies in the heterogeneous distribution of atomic activation energies on different crystal planes: the atomic removal probability is inversely proportional to the activation energy. Crystal planes with high etching rates exhibit lower overall activation energies, while those with low etching rates exhibit higher overall activation energies. Furthermore, P atoms are more readily removed by etching than In atoms, which also explains the difference in etching rates between the two opposite sides of the (111) plane. The relative errors between the simulated etching rates of various typical crystal planes and the experimental measurements are all within 8%. The simulated three-dimensional etching morphologies for masks of different shapes are in perfect agreement with the experimentally observed macroscopic structures, sidewall angles, and corner rounding features. These results demonstrate that the InP-

© 2026 by the author(s). Distributed under a Creative Commons CC BY license.

EMC etching simulation model constructed in this study can accurately predict the wet etching process of InP under arbitrary mask structures, providing a reliable theoretical support for the micro/nano-fabrication process design of InP-based optoelectronic devices. This work was supported by the Qinglan Project for Outstanding Young Teachers of Jiangsu Province (Grant No. 202050225RS003) and the Open Research Fund of the Jiangsu Provincial Engineering Research Center for Industrial Perception and Intelligent Manufacturing Equipment (Grant No. ZK22-05-07).

## References


1. D. D. Van *et al.*, "Epitaxial Defects in Nanoscale InP Fin Structures Revealed by Wet-Chemical Etching," *Crystals,* vol. 7, no. 4, p. 98, 2017.
2. Z. Weng *et al.*, "Selective etching of InP in NaF solution," *Applied Surface Science,* vol. 256, no. 7, pp. 2052-2055, 2010.
3. K. V. S. R. Kishore, N. K. Vangala, A. Dasgupta, and N. Dasgupta, "Effect of Etch Mask and Etching Solution on InP Micromachining to Form V-Grooves," *Journal of the Electrochemical Society,* vol. 148, no. 4, pp. C322-C326, 2001.
4. W. Guo *et al.*, "KOH based selective wet chemical etching of AlN, AlxGa1xN, and GaN crystals: A way towards substrate removal in deep ultraviolet-light emitting diode," *Applied Physics Letters,* vol. 106, no. 8, p. 1594, 2015.
5. C. W. Park, J. H. Park, Y. P. Hong, D. K. Oh, and K. B. Shim, "Wet chemical etching of molten KOH/NaOH eutectic alloy to evaluate AlN single crystal," *Journal of the Korean Crystal Growth and Crystal Technology,* vol. 24, no. 6, pp. 237-241, 2014.
6. L. Weiwei, Z. Youwen, D. Zhiyuan, Y. Jun, H. Weijie, and K. Jianhong, "Wet etching and infrared absorption of AlN bulk single crystals," *Journal of Semiconductors,* vol. 30, no. 007, p. 073002, 2009.
7. S. Dutta, M. Imran, P. Kumar, R. Pal, P. Datta, and R. Chatterjee, "Comparison of etch characteristics of KOH, TMAH and EDP for bulk micromachining of silicon (110)," *Microsystem Technologies,* vol. 17, no. s 10-11, pp. 1621-1628, 2011.
8. M. A. Gosálvez, P. Pal, N. Ferrando, H. Hida, and K. Sato, "Experimental procurement of the complete 3D etch rate distribution of Si in anisotropic etchants based on vertically micromachined wagon wheel samples," *Journal of Micromechanics and Microengineering,* vol. 21, no. 12, p. 125007, 2011.
9. M. A. Gosálvez, P. Pal, and K. Sato, "Reconstructing the 3D etch rate distribution of silicon in anisotropic etchants using data from vicinal {1 0 0}, {1 1 0} and {1 1 1} surfaces," *Journal of Micromechanics & Microengineering,* vol. 21, no. 10, p. 105018, 2011.
10. N. Ferrando, M. A. Gosálvez, and R. J. Colóm, "Evolutionary continuous cellular automaton for the simulation of wet etching of quartz," *Journal of Micromechanics and Microengineering,* vol. 22, no. 2, Feb 2012, Art no. 025021. https://doi.org/10.1088/0960-1317/22/2/025021.
11. H. Zhang, J. Qian, and L. L. Hong, "Etching conditions effect on anisotropic properties of sapphire," *Journal of Crystal Growth,* vol. 622, Nov 2023, Art no. 127402. https://doi.org/10.1016/j.jcrysgro.2023.127402.
12. Y. Xing, Z. Y. Guo, M. A. Gosálvez, G. R. Wu, and X. L. Qiu, "Characterization of anisotropic wet etching of single-crystal sapphire," *Sensors and Actuators a-Physical,* vol. 303, Mar 2020, Art no. 111667. https://doi.org/10.1016/j.sna.2019.111667.
13. D. T. Lowes, "Photochemical etching of n-InP," *Cassidy D T,* 1991.
14. P. P. Notten, "The Etching of InP in HCl Solutions: A Chemical Mechanism," *Journal of The Electrochemical Society,* vol. 131, no. 11, pp. 2641-2644, 1984.
15. H. K. Sadao Adachi, " Chemical Etching Characteristics of ( 001 ) InP," *Journal of The Electrochemical Society,* vol. vol. 128, pp. 1342- 1349, 1981.
16. M. Kappelt and D. Bimberg, "WET CHEMICAL ETCHING OF HIGH QUALITY V-GROOVES WITH (111) A SIDEWALLS ON (001) INP," *Journal of the Electrochemical Society,* 1996.
17. D. W. P. Bönsch, T. Schrimpf, A. Schlachetzki, R. Lacmann, "Ultrasmooth V-Grooves in InP by Two-Step Wet Chemical Etching," *Journal of The Electrochemical Society,* vol. 145, pp. 1273- 1276, 1998.
18. A. Mouton, C. S. Sundararaman, H. Lafontaine, S. Poulin, and J. F. Currie, "Etching of InP by H3PO4, H2O2 Solutions," *Japanese Journal of Applied Physics,* vol. 29, no. Part 1, No. 10, pp. 1912-1913, 1990.


© 2026 by the author(s). Distributed under a Creative Commons CC BY license.

Preprints.org (www.preprints.org) | NOT PEER-REVIEWED | Posted: 6 May 2026 doi:10.20944/preprints202605.0264.v1




19. R. Klockenbrink, E. Peiner, H. H. Wehmann, and A. Schlachetzki, "Wet chemical etching of alignment V-grooves in (100) InP through titanium or In(0.53)Ga(0.47)As masks," *Journal of the Electrochemical Society*, vol. 141, no. 6, pp. 1594-1599, 1994.
20. H. Zhang, Y. Xing, M. A. Gosálvez, P. Pal, and K. Sato, "Removal probability function for Kinetic Monte Carlo simulations of anisotropic etching of silicon in alkaline etchants containing additives," *Sensors and Actuators a-Physical*, vol. 233, pp. 451-459, Sep 2015. https://doi.org/10.1016/j.sna.2015.07.031.
21. Y. Xing, M. A. Gosálvez, K. Sato, M. Tian, and H. Yi, "Evolutionary determination of kinetic Monte Carlo rates for the simulation of evolving surfaces in anisotropic etching of silicon," *Journal of Micromechanics and Microengineering*, vol. 22, no. 8, Aug 2012, Art no. 085020. https://doi.org/10.1088/0960-1317/22/8/085020.


**Disclaimer/Publisher's Note:** The statements, opinions and data contained in all publications are solely those of the individual author(s) and contributor(s) and not of MDPI and/or the editor(s). MDPI and/or the editor(s) disclaim responsibility for any injury to people or property resulting from any ideas, methods, instructions or products referred to in the content.

© 2026 by the author(s). Distributed under a Creative Commons CC BY license.